Stem Cell Reports
Article

ISSCR

OPEN ACCESS

Cell position within human pluripotent stem cell colonies determines apical specialization via an actin cytoskeleton-based mechanism

Youngju Kim,[1] Hwanseok Jang,[2] Kyubin Seo,[1] June Hoan Kim,[1] Boram Lee,[1] Hyo Min Cho,[1] Hyun Jung Kim,[1] Esther Yang,[1] Hyun Kim,[1] Jeong-An Gim,[3] Yongdoo Park,[2] Jae Ryun Ryu,[1,*] and Woong Sun[1,*]

[1]Department of Anatomy, Korea University College of Medicine, 73 Inchon-ro, Seongbuk-gu, Seoul 02841, Republic of Korea
[2]Department of Biomedical Sciences, Korea University College of Medicine, 73 Inchon-ro, Seongbuk-gu, Seoul 02841, Republic of Korea
[3]Medical Science Research Center, College of Medicine, Korea University Guro Hospital, 148 Gurodong-ro, Guro-gu, Seoul 08308, Republic of Korea
*Correspondence: jaeryunryu@gmail.com (J.R.R.), woongsun@korea.ac.kr (W.S.)
https://doi.org/10.1016/j.stemcr.2021.11.005

SUMMARY

Human pluripotent stem cells (hPSCs) grow as colonies with epithelial-like features including cell polarity and position-dependent features that contribute to symmetry breaking during development. Our study provides evidence that hPSC colonies exhibit position-dependent differences in apical structures and functions. With this apical difference, edge cells were preferentially labeled with amphipathic dyes, which enabled separation of edge and center cells by fluorescence-activated cell sorting. Transcriptome comparison between center and edge cells showed differential expression of genes related to apicobasal polarization, cell migration, and endocytosis. Accordingly, different kinematics and mechanical dynamics were found between center and edge cells, and perturbed actin dynamics disrupted the position-dependent apical polarity. In addition, our dye-labeling approach could be utilized to sort out a certain cell population in differentiated micropatterned colonies. In summary, hPSC colonies have position-dependent differences in apical structures and properties, and actin dynamics appear to play an important role in the establishment of this position-dependent cell polarity.

INTRODUCTION

Human pluripotent stem cells (hPSCs) are unique cells that are capable of infinitely proliferating into the same type of cells in defined *in vitro* culture conditions (self-renewal) and can form three germ layers and further differentiate into virtually all types of somatic cells in humans (Romito and Cobellis, 2016; Thomson et al., 1998). Initially homogeneous hPSCs are spatiotemporally controlled during development and produce organized tissue architectures (self-organization). In patterning and morphogenesis via self-organization of stem cells, symmetry breaking is an essential step and is closely associated with cell polarity (Simunovic and Brivanlou, 2017). The polarized structure of hPSCs originates from their epithelial cell-like properties. They tightly adhere to each other while establishing polarity (Krtolica et al., 2007). This polarity is generally characterized by apical, lateral, and basal plasma membrane domains, which are composed of differential distributions of phospholipids, protein complexes, and cytoskeletal components (Florian and Geiger, 2010). As cells grow *in vitro* in tightly packed colonies, hPSCs exhibit different features of polarity depending on their location in the colony (position dependency). For instance, cells at the edge of the colony have a different relationship with neighboring cells, and these edge cells often exhibit different aspects of cell polarity, such as enhanced basal attachments and the formation of ventral stress fibers with focal adhesion (FA) representing basolateral specialization (Närvä et al., 2017; Stubb et al., 2019).

These topological differences in cell polarization in colonized cells appear to influence cellular physiology and fate specification (Etoc et al., 2016; Heemskerk and Warmflash, 2016; Ma et al., 2015), and by strengthening this feature with geometric confinement of the cells in an arena coated with defined extracellular matrix molecules, hPSC differentiation can be patterned into three germ layer-like alignments (Warmflash et al., 2014), depending on cell location. There are several models explaining how these differences emerge from topological differences of the cells (Deglincerti et al., 2016a), which include the differential expression of morphogens or their receptors (Etoc et al., 2016), different cell shape, and cytoskeletal contractile force (Xue et al., 2018). However, despite the biological importance of cell position and polarity for fate determination, the precise mechanisms of how, and how much cell position within colony affects cellular determination remain elusive. At least one factor impeding the understanding of these and related issues is the absence of suitable tools to isolate center and edge cells for unbiased biochemical or -omics study.

In this study, we discovered that edge cells failed to establish structural apicalization of protein distribution, villi-like protrusions, and glycocalyx formation, all of which are well displayed in center cells. Furthermore, several vital dyes widely used for the labeling of subcellular organelles such as nuclei, mitochondria, and cell membranes, stained hPSC colonies in a position-dependent manner. By use of these dyes, hPSCs can be separated into two populations depending on their original position in a colony, and we

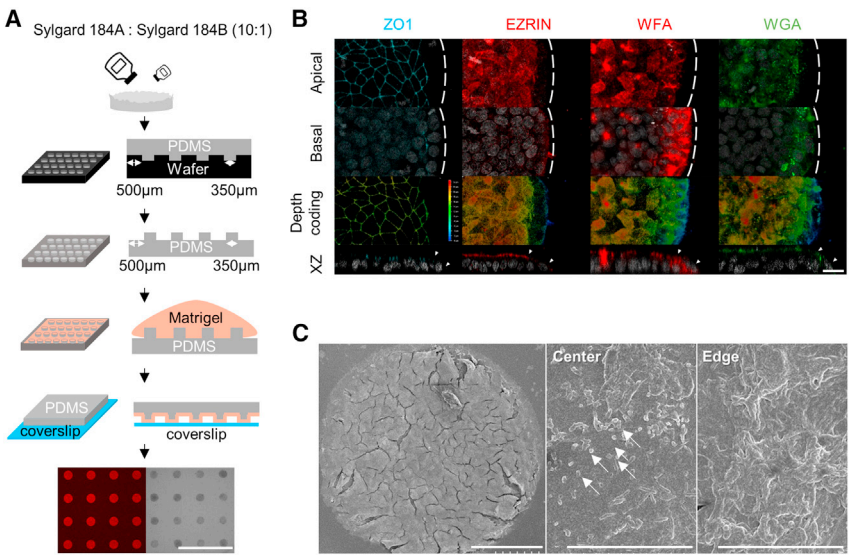

Figure 1. Apical characteristics of edge and center cells in a micropatterned hPSC colony

(A) A procedure for micro-contact printing. A polydimethylsiloxane stamp with micropatterns was covered with Matrigel and coated overnight at 4°C. Then, the stamp was placed on the coverslip for 10 min. Immediately thereafter, stamps were removed and cells were seeded on coverslips. Scale bar, 2,000 μm.

(B) Localization of apical specialization proteins in hPSC colony. Confocal images were taken in 1-μm steps along the z axis. "Apical" images were generated by stacking images from the top of the edge of the cell nucleus to the top of apical proteins of center cells (approximately 13 μm) and "Basal" images from the very bottom to the end of the apical (approximately 16 μm) using z stack maximum projection. Depth coding indicates the apical side in red and the bottom side in blue. Images of side view (XZ) are displayed. Scale bar, 20 μm.

(C) Ultrastructure of the surface of micropatterned H9 cell colony was examined by SEM. Scale bars, 100, 50, and 5 μm (from left). The protrusions on the surface of center cells are highlighted with arrows.

were able to explore position-dependent gene expression profiles. This study provides unbiased identification of position-dependent gene expression patterns, which improve understanding of the cell specification and patterning of stem cells.

RESULTS

Position-dependent apical specialization in hPSC colonies

Because the size, shape, and density of colonies are difficult to control in normal and conventional cell culture, the mechanical forces and topological relationship of the cells in the colony are inhomogeneous (Orozco-Fuentes et al., 2019). To reduce the heterogeneity of the hPSC colony and for ease of analyses, we employed a micropattern-based cell culture (Figure 1A), which allowed the precise control of the size and shape of the cell colony (Théry, 2010). hPSCs grown on micropatterns maintained expression of pluripotency marks, including OCT4, SOX2, and NANOG, and these markers were uniformly expressed in all the positions within the colony (Figure S1A). In micropatterned hPSC colonies, highly polarized tight junction protein ZO1 was found at the apical-lateral domain of the cells in the center of the colony, but not at the outer face of the edge cells (Figure 1B) due to the absence of neighbors (Etoc et al., 2016). Also, the apical marker protein EZRIN was exclusively found at the apical domain of the center cells, but not at the edge cells. Lectins recognizing the glycans at the cell surfaces also exhibited differential distribution depending on position within the colony; wheat germ agglutinin (WGA), a lectin that binds to N-acetyl-D-glucosamine and sialic acid (Monsigny et al., 1980; Reily et al., 2019), localized at the apical domain of the center cells, as demonstrated previously (Etoc et al., 2016). With more detailed analysis, we also observed that WGA was preferentially located at the basal region of the edge cells. Similarly, *Wisteria floribunda* agglutinin (WFA) lectin, which binds to N-acetyl galactosamine beta1 of glycoproteins (Hilbig et al., 2001), also exhibited apical localization in the center cells, but basolateral distribution in the edge cells (Figure 1B). In addition to the membrane-associated lectin signals, many punctiform signals were especially enriched in the cytosol, suggesting that they are a fraction of the membrane internalized by endocytosis. Double labeling with early endosome marker EEA1 confirmed that at least a sub-fraction of these were included in the early endosome via endocytosis (Figure S1B).

The ultrastructural differences in the apical domain depending on cell position within colony were also addressed with scanning electron microscopy (SEM). While cells at the center exhibited villi-like protrusions at the apical surface, edge cells exhibited lamellipodia-like ruffles at their surface, providing evidence that specialization of apical structures is influenced by cell position (Figure 1C).

Permeable dye diffusion patterning in hPSC colonies

In addition to the structural differences in apical specialization depending on cell position, live cell labeling of the

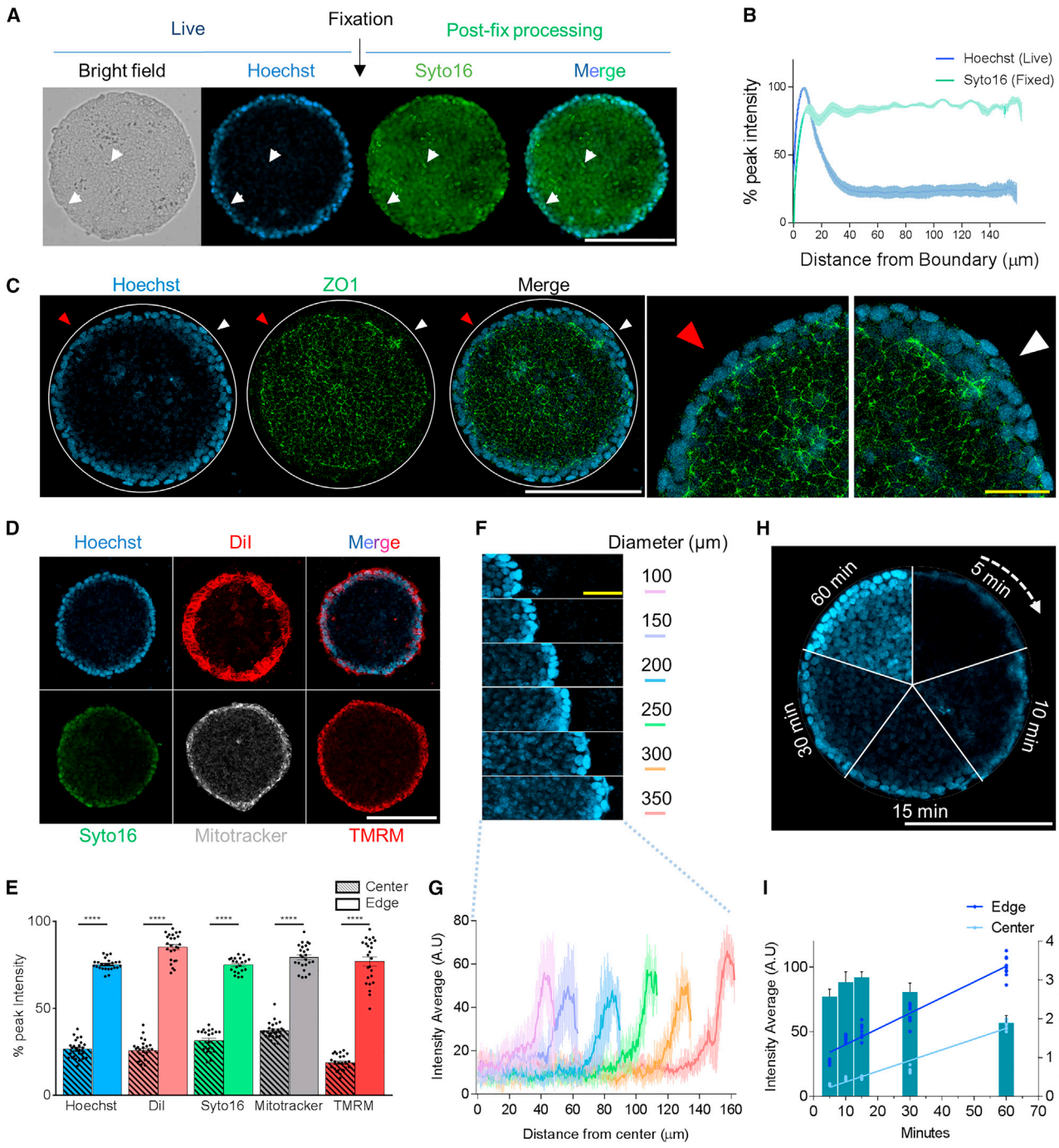

Figure 2. Live labeling of hPSCs cultured on micropattern with fluorescence dyes

(A) hPSCs were seeded onto the micropattern and live cells were labeled with Hoechst 33342. After bright-field and fluorescent images were taken in live cells, cells were fixed and labeled with Syto16. Hoechst 33342 images from live cells and Syto16 images from fixed cells were merged. Arrowheads indicate mitotic cells. Scale bar, 200 μm.

(B) Dye-labeling intensity at each region in the colony was divided by the highest intensity in the same colony for normalization, and the value was converted to the percent peak. Data represent the mean ± SEM (n = 10 colonies, three independent experiments).

(C) Fluorescence live imaging of PSCs expressing EGFP-ZO1 upon Hoechst labeling. Edge area varies depending on the region. Triangles indicate edge area is within one cell layer (white) or two cell layers (red) of micropattern boundary. Scale bars, 200 μm (white) and 50 μm (yellow).

(legend continued on next page)

hPSCs with Hoechst 33342 showed that, one to two cell layers from the edge, "edge cells" hereafter, were more strongly labeled than the center cells (Figure 2A). This difference appeared to be strongly associated with cell location, but not with cell cycle, since mitotic cells exhibiting chromosome condensation at the edge or center faithfully exhibited dye-labeling intensity similar to their neighbor cells (Figure 2A, arrowheads). Labeling of nuclei with Syto16 after fixation demonstrated that the labeling intensity was even regardless of cell position, indicating that the center-edge difference is not dependent on cell density (Figures 2B and S3A) or DNA content in each cell, but on the biological activity of the cells at their position. To examine whether higher dye labeling at the edge was due to non-homogenous substrate printing within the micropattern, we immunostained the Matrigel substrate with anti-laminin and anti-collagen type IV antibodies after micro-contact printing. Extracellular matrix (ECM) molecules were not adsorbed, especially highly at the edge of the pattern although stronger adsorption spots were randomly observed; and these spots did not seem to be related with high dye labeling. As more uniform adsorption of ECM was obtained using a stencil micropatterning system, a dye-labeling experiment was repeated in a stencil system, and differential dye labeling at edge and center cells was consistently observed (Figure S2). Therefore, we were able to exclude the possibility that stronger dye labeling in edge cells of embryonic stem cell colonies is due to the greater ECM deposits during the micropatterning procedure. Next, we explored whether apical-basal polarity was associated with the live dye-labeling profile in micropatterned colonies. We used the hPSCs stably expressing EGFP-ZO1 and performed live imaging after dye labeling. As shown in Figure 2C, the edge region with higher dye labeling was completely the same as the region without polarized ZO1. The dye-labeled edge area exhibited variations (within one or two cell layers of micropattern boundary) depending on the region which was marked with white (one cell layer) and red (two cell layer) triangles, while clear correlation between apical-basal polarity and spatial profile of dye labeling was maintained (Figure 2C).

Other dyes, including 1,1′-dioctadecyl-3,3,3′,3′-tetramethylindocarbocyanine (DiI), Syto16, MitoTracker (M22426), and tetramethylrhodamine methyl ester (TMRM), which have different chemical characteristics, also showed similar features, i.e., strong edge labeling, when they were added to the live cell colony (Figures 2D and 2E). In particular, DiI is a lipophilic dye that forms fine aggregates in media, and is widely used for membrane labeling of cells, because it adheres to the cell membrane and freely diffuses along the attached cell membrane but not to other cells. Accordingly, 5 min after DiI incubation, DiI crystals were randomly precipitated, with weak diffusion of fluorescence only at the edge. By 15 min after incubation, DiI diffusion was prominent only at the edge, while dye diffusion was only marginal at the center, suggesting that the diffusion of this dye to the cell membrane is position dependent (Figure S3B).

To further characterize position-dependent dye labeling, we examined whether different colony size as controlled by micropattern diameter affected dye-labeling features. In all the different sizes of micropatterns (from 100 to 350 μm with 50-μm increments), edges with uniform length from the boundary were distinguishable by strong dye labeling (Figures 2F and 2G). Time course analysis with Hoechst further revealed that differential dye labeling was evident immediately after incubation and maintained at least up to an hour (Figure 2H). Linear regression analysis demonstrated that the kinetics of dye labeling at the center and edge were similar (Figure 2I). Furthermore, colonies of different hPSC lines in normal or micropattern culture conditions exhibited noticeable distinctions between center and edge by differential dye-labeling and apical marker staining, suggesting that this phenomenon is a universal and fundamental feature of hPSC colonies (Figure S3C).

Taken together, these data suggest that the differences between the two areas may be associated with simple

(D) Various dye labeling in an hPSC colony. Live cells were simultaneously stained with Hoechst 33342 and DiI, and images were merged. Live cells were labeled with Syto16, Mitotracker, or TMRM. Scale bar, 200 μm.

(E) Quantification of center and edge cell dye intensity in (D). Dye intensity of edge and center cells were measured and percent peak intensity was calculated. The length of the edge was defined as 12.3 ± 0.73 μm (mean ± SEM). Each dot represents percent peak intensity of an individual colony randomly collected in three independent experiments (n = 26–30). ****$p < 0.0001$ from t test.

(F) The effect of colony size on dye labeling in an hPSC colony. The size of the hPSC colony was regulated by micropattern diameter. Scale bar, 50 μm.

(G) Quantification of dye-labeling intensity in (F) (n = 9 colonies, three independent experiments). Data represent the mean ± SEM. AU, arbitrary units.

(H) Dye diffusion kinetics at the edge and center of the colony. Fluorescent images of the Hoechst 33342-labeled colony were taken at 5, 10, 15, 30, and 60 min after dye addition. Temporal order of images is presented in a clockwise direction. Scale bar, 200 μm.

(I) Quantification of dye intensity and ratio of edge to center in (H). Left: y axis with line graphs indicates the intensity (AU, arbitrary units). Each dot represents average intensity of edge or center cells. Right: y axis with the bar graphs indicates intensity ratio of edge to center (n = 10 colonies, three independent experiments). Data represent mean ± SEM.

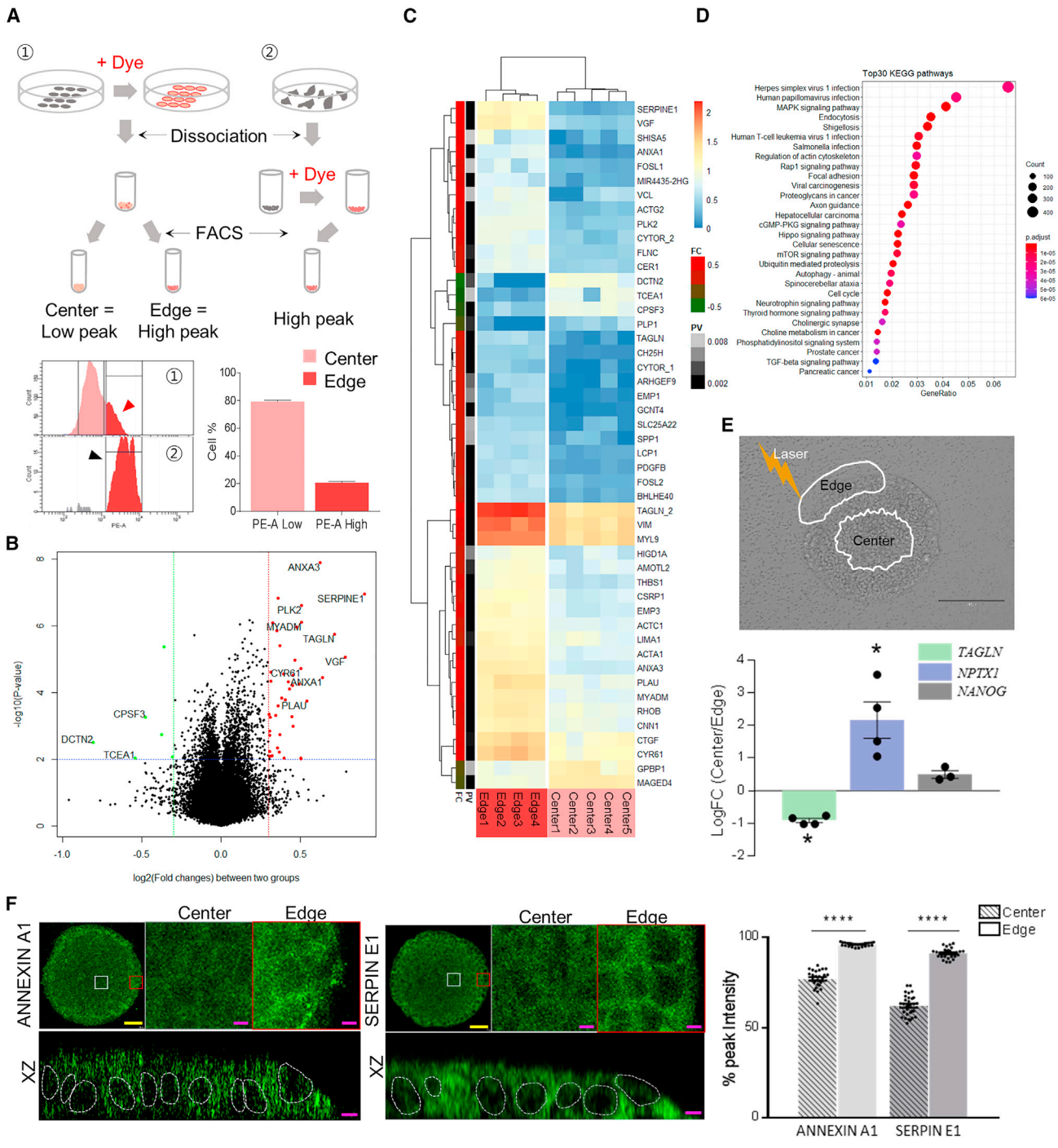

Figure 3. Separation of edge and center cells by FACS and RNA-seq analysis

(A) To isolate edge and center cells for mRNA sequencing, micropatterned hPSC colonies were labeled with TMRM for 15 min at 37°C and dissociated as single cells. Low- and high-intensity populations were separated by FACS analysis (①). To clarify the high-intensity peak, dissociated single cells were also labeled with TMRM for 15 min at 37°C and analyzed (②). The high-intensity populations from micropatterned colonies (marked with red arrowhead) was overlapped with the single-cell TMRM-labeled population (marked with the black arrowhead). The quantification graph shows each cell population as a percentage (n = 5). Data represent the mean ± SEM.

(B) Volcano plot shows fold change versus p value. Significant DEGs were selected when the fold change (FC) value gap was higher than 1.2 and $p < 0.01$. Genes higher expressed in the edge are colored red, whereas lower expressed genes are colored green.

(legend continued on next page)

differences of dye permeability/diffusion. One alternative possibility is that the center cells display higher dye efflux mediated by multiple drug-resistant (MDR) ATPase transporters (Lahmy et al., 1995; Zhou et al., 2001). However, treatment with inhibitors against major MDR ATPase transporters did not interfere with the center-edge difference, and it is unlikely that differences in efflux capacity between edge and center cells mediates the differential dye labeling in hPSC colonies (Figures S3D and S3E).

Unbiased comparison of differential gene expression dependent on cell position

Position-dependent dye labeling within micropatterned colonies allowed the separation of cells depending on their cell position by fluorescence-activated cell sorting (FACS), which enabled further biochemical analysis with purified cell populations. Thus, cells were grown on arrays of 350 μm diameter micropatterns, labeled with TMRM, dissociated, and subjected to FACS. Low and high peaks were obtained with FACS analysis of dissociated micropatterned cells. To define high-intensity peak consistently in every experiment, PSC colonies were dissociated into single cells without any cellular contact and then labeled with TMRM. Fluorescence peaks from labeled single cells were always overlapped with the high fluorescence peaks of micropatterned cells. This procedure successfully separated center cells with low TMRM intensity and edge cells with high TMRM intensity (Figure 3A). We compared the percentage of edge cells at the micropatterned colony with that of higher labeling cells from FACS analysis to assure they were the same population. Edge cells were located within approximately 20 μm of the micropattern boundary, and therefore the surface area occupied by edge cells is 75,438.5 μm^2, which means that the percentage of edge cells is calculated as 21.55%. Our FACS analysis data showed that the percentage of cells with higher intensity peak is 20.68% ± 0.99%. Accordingly, the edge proportion calculated from the micropattern colony is approximately the same as that from FACS analysis. However, to clearly separate edge cells from center cells, only the brightest 10% of cells with high intensity (edge cells) were used in the analysis.

From each population, RNA was purified and RNA-seq analyses were executed to compare the differential gene expression. Volcano plots showed that the expression level of 48 genes significantly differed between the two groups (42 genes were high in the edge, and 6 genes were low in the edge cells, as compared with the center; Figure 3B, and the full list of genes is shown in Table S1). Genes higher expressed in the edge are colored as red in the volcano plot, and they included actin-related genes. The heatmap of 48 differentially expressed genes (DEGs) was generated across center (5 samples) and edge (4 samples) cells. Nine samples were clearly divided into the two groups by hierarchical clustering analysis (Figure 3C), suggesting that the cell separation was successful and that the transcriptome profiles in each group share similarities in their gene expression patterns.

Then, gene-enrichment and functional annotation analysis was performed using KEGG and gene ontology (GO). KEGG analyses demonstrated that DEGs in this comparison were associated with biological pathways, including endocytosis and FA. Lists of the top 30 KEGG categories by DEGs are depicted as dot plots in Figure 3D. GO enrichment analysis also revealed that the enriched DEGs were associated with migration-related processes under biological process GO terms, and associated with FA, filopodium, and actin-related components under cellular component GO terms (Figure S4). To confirm DEG profile from RNA-seq data using FACS-sorted edge and center cells in micropatterned colonies, we isolated edge and center cells using a laser-capture microdissection technique (Podgorny, 2013), and quantified the expression levels of *NPTX1*, *TAGLN*, and *NANOG* with qPCR. The *NPTX1* gene was chosen as a representative gene of center-enriched genes, and *TAGLN* was chosen among edge-enriched genes. *NANOG* was used as a uniformly expressing gene at the center and edge cells. In consistence with RNA-seq data, qPCR data

(C) Heatmap of 48 genes that are differentially expressed between the edge and center cell groups (edge sample, n = 4; center sample, n = 5). Six genes were highly expressed in the center (green annotation bar) and 42 genes at the edge (red annotation bar). The grayscale annotation bar represents statistical significance between edge and center.

(D) KEGG enrichment analyses are depicted as a dot plot. DEGs were annotated and the top 30 pathways were selected.

(E) Verification of RNA-seq data. Edge and center cells cultured on micropatterned polyethylenenaphthalate membrane were cut using a laser under LCM. The white line indicates a cutting margin (top). Scale bar, 150 μm. Ten to 15 colonies were cut and collected from each experiment, and four independent experiments were performed. qPCR data from collected edge and center cells (bottom). FC (center/edge) of indicated genes was calculated, and the ΔCT values of center and edge cells for each gene were used for statistical analysis. Data represent mean ± SEM. Each dot represents fold change of an individual batch of experiment (n = 3 or 4). *p < 0.05 from t test.

(F) Validation of RNA-seq data by immunostaining of ANNEXIN A1 and SERPIN E1. Both proteins were highly expressed in edge cells and polarized in distribution. Data represent mean ± SEM (right side). Each dot represents percent peak intensity of an individual colony randomly collected in three independent experiments (n = 26–30). ****p < 0.0001 from t test. Scale bars, 20 μm (yellow) and 5 μm (magenta).

showed that the *TAGLN* level in edge cells is two times higher than those in center cells, and the *NPTX1* level in edge cells is five times lower than in center cells, while the *NANOG* level remained similar in both positions (Figure 3E). The fluorescence *in situ* hybridization technique also showed that *NPTX1* was expressed more in center cells and *TAGLN* more in edge cells, while *POLR2A* was uniformly expressed at both cells similar to *NANOG* (Figure S5). These data confirmed that edge cells in the micropatterned colonies were the same cells displaying high peak at FACS analysis. To validate the result obtained from the RNA-seq data at a protein level, we chose two genes, Annexin A1 (*ANXA1*) and Serpin E1 (*SERPINE1*), and found that they were enriched in the edge cells, which is consistent with the RNA-seq data (Figure 3F). Interestingly, ANNEXIN A1 was enriched at the apical side of the center cells, and SERPIN E1 at the apicolateral side in the center cells. On the contrary, both proteins were preferentially distributed at the basolateral side in the edge cells. These results indicated that not only the amount but also the distribution of these proteins, are controlled by cell position within colony.

Location dependence of the movement and physical force of cells within the hPSC colony

Our DEG analysis revealed that several classes of genes related to cell migration and cellular movement were significantly increased in the edge cells. Supporting our data, the previous study also showed that edge cells in hPSC colonies exhibit distinct actin organization and stronger traction force (Rosowski et al., 2015). Therefore, we examined kinematics and mechanical dynamics in hPSC colonies. Cell trajectories, which were quantified by cell images obtained over 24 h, created a swirl pattern, and, notably, cells located at the edge showed the longest mobility (Figure 4A). In addition to the moving distance, cells located within 20 μm of the edge showed twice the speed as those located in the center of the colony (Figure 4B). Analysis of cellular physical forces during cell migration can elucidate the mechanical interactions of cells that cannot be defined by conventional biological analysis. The traction force exerted by the cells on the substrate showed an isotropic distribution balance within the colony (Figure 4C). In particular, through the traction force with a central direction appearing in cells at the edge, the cells migrated in a circumferential direction along the trapped area instead of moving outward. At the edge of the colony, where the traction force in a central direction was relatively weak, the tension, indicating the physical stress with a normal direction between cells, was also shown to be weak: below 150 Pa (Figure 4D). This implies that the cells located in the center showing low motility are connected through strong tension, while the cells located at the edge showing active individual motility have a weak connection with their neighbor cells. Taken together, our results revealed that the hPSC colony showed differential kinematics and mechanical dynamics depending on location within a confined area on the micropattern.

Actin dynamics are critical for apical specialization and position-dependent dye diffusion

The above RNA-seq analyses suggested that the actin dynamics-related apicobasal axis formation is responsible for the establishment of center-edge formation. Thus, the effect of perturbation of actin dynamics using ROCK inhibitor Y27632 on differential apical features between the center and edge was assessed. Treatment of hPSC colonies with Y27632 for 24 h prior to dye incubation substantially increased Hoechst 33342 and DiI labeling intensities in center cells (Figure 5A). While there were significant variations among the cell colonies, it appeared that there was a tendency for Y27632 treatment to expand the strong dye-labeling area toward the center from the colony edge. Y27632 treatments also disrupted polarized distribution of apicolateral indicator ZO1 and apical specialization markers such as WFA, WGA, and EZRIN in the center cells (Figure 5A). Similar to ROCKi, specific actin assembly inhibitors, cytochalasin D and latrunculin B, changed dye-labeling profile in micropatterned cells and simultaneously disrupted tight junction (Figure S6). Thus, it appears that proper actin polymerization is required for the establishment/maintenance of core-edge segregation.

The effect of Y27632 treatment on distribution of ANNEXIN A1 and SERPIN E1 was examined (Figure 5B). ANNEXIN A1, which was located preferentially at the apical side in the center cells, redistributed toward the lateral side with Y27632 treatment while actin disruption showed no significant differences in the edge cells. SERPIN E1 also showed a similar pattern of changes as actin disruption, although the change was not as evident as in ANNEXIN A1. Interestingly, the redistribution to the lateral side among center cells as shown in Figure 5B was observed in apical markers, WGA and EZRIN, after Y27632 treatment (Figure S7), indicating that center cells might gain edge-like properties including absence of apical polarization. These results supported the notion that positional differences in apical specialization and dye penetration pattern in hPSC colonies are regulated by actin cytoskeletal dynamics.

Finally, we tested whether core-edge relationship is maintained in micropatterned colonies upon differentiation. Micropatterned PSC colonies were treated with Wnt3a and Activin A to differentiate them into regionally defined ectoderm-endoderm lineages (Martyn et al., 2018), and labeled with Hoechst 33342 dye after 24 h. Cells close to the periphery (three to five cells in length) were labeled

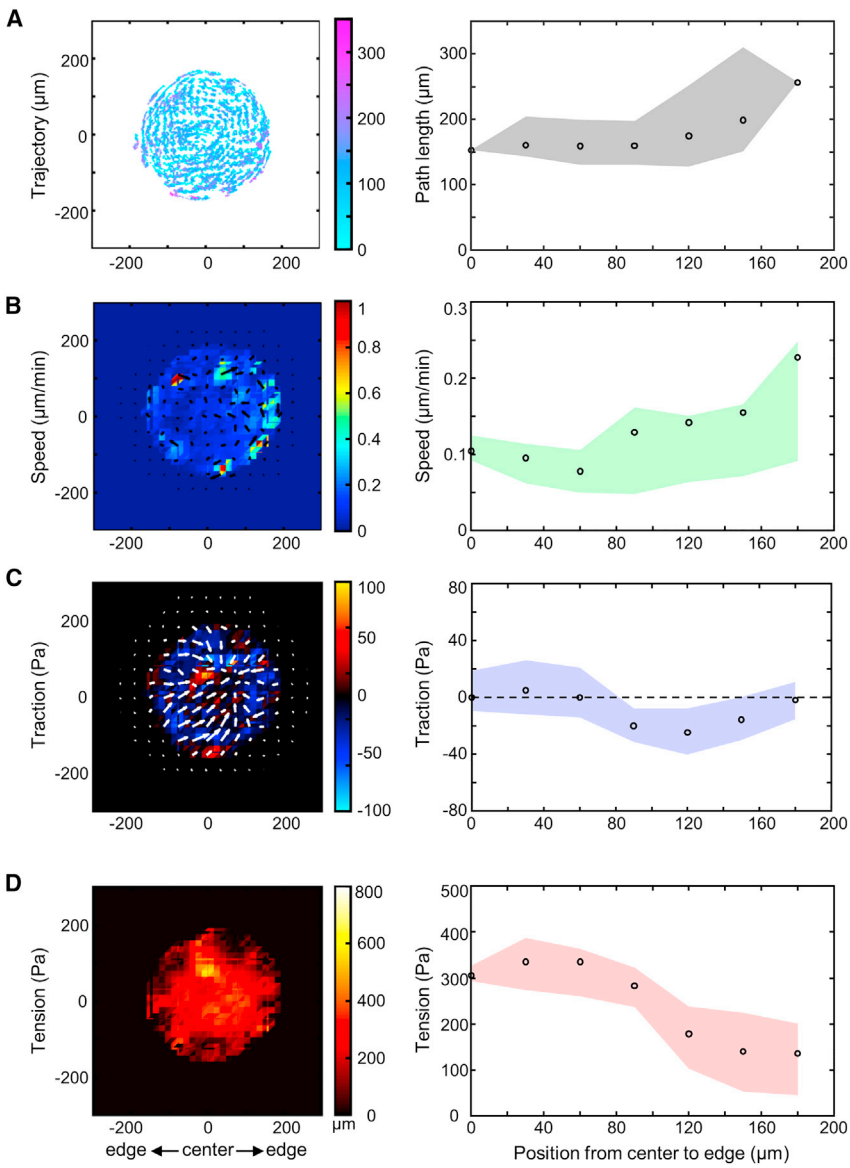

Figure 4. Differential kinematics and mechanical dynamics in an hPSC colony

(A) Cell trajectory with a path length indicated by a purple gradient (left) and the mean path lengths (black circles) and mid-quartile (gray) obtained along the radial lines from the center to the edge of the cell colony for 24 h (right).

(B) A color-coded map of cell speed with migration direction (black arrows) (left) and the mean speed (black circles) and mid-quartile (green) obtained along the radial lines from the center to the edge of the cell colony (right) at 60 min.

(C) A color-coded map of radial coordinated cellular traction force with traction direction (white arrows) (left) and the mean traction (black circles) and mid-quartile (blue) obtained along the radial lines from the center to the edge of the cell colony (right) at 60 min.

(D) A color-coded map of tension (left) and the mean tension (black circles) and mid-quartile (red) obtained along the radial lines from the center to the edge of the cell colony (right) at 60 min. All the data for the analysis of distribution of cellular migration was obtained from the number of data points with a size of 64 × 64 points (n = 732) acquired from center to edge.

significantly higher than cells inside in differentiated micropatterned colonies. When fixed cells were immunostained with various early differentiation markers, those cells with higher dye labeling were SOX17-positive endodermal cells (Figure 5C). Next, we examined whether these different cell types after differentiation could be sorted by FACS based on dye labeling. Differentiated cells were sorted into two populations as shown in Figure 5D. qPCR using sorted cells revealed that, consistent with immunofluorescence data, mRNA levels of the definitive endoderm markers, *SOX17* and *MIXL1* (Green et al., 2011), were higher in the higher labeling population than the lower labeling population.

On this differentiation condition, tight junctions were globally disrupted, and with no clear edge-core differences in the colony, suggesting that these differences in dye labeling are more likely associated with cell-type-dependent features of dye permeability. Regardless of the precise mechanism, this result also suggested that our dye-labeling method can be used to isolate a certain cell population from other cell types in micropatterned PSCs during differentiation.

DISCUSSION

We and others have shown that hPSC colonies have position-dependent differences in structures and functions of cells. It has been reported that differential presentation of receptor proteins and gradients of humoral factors, in

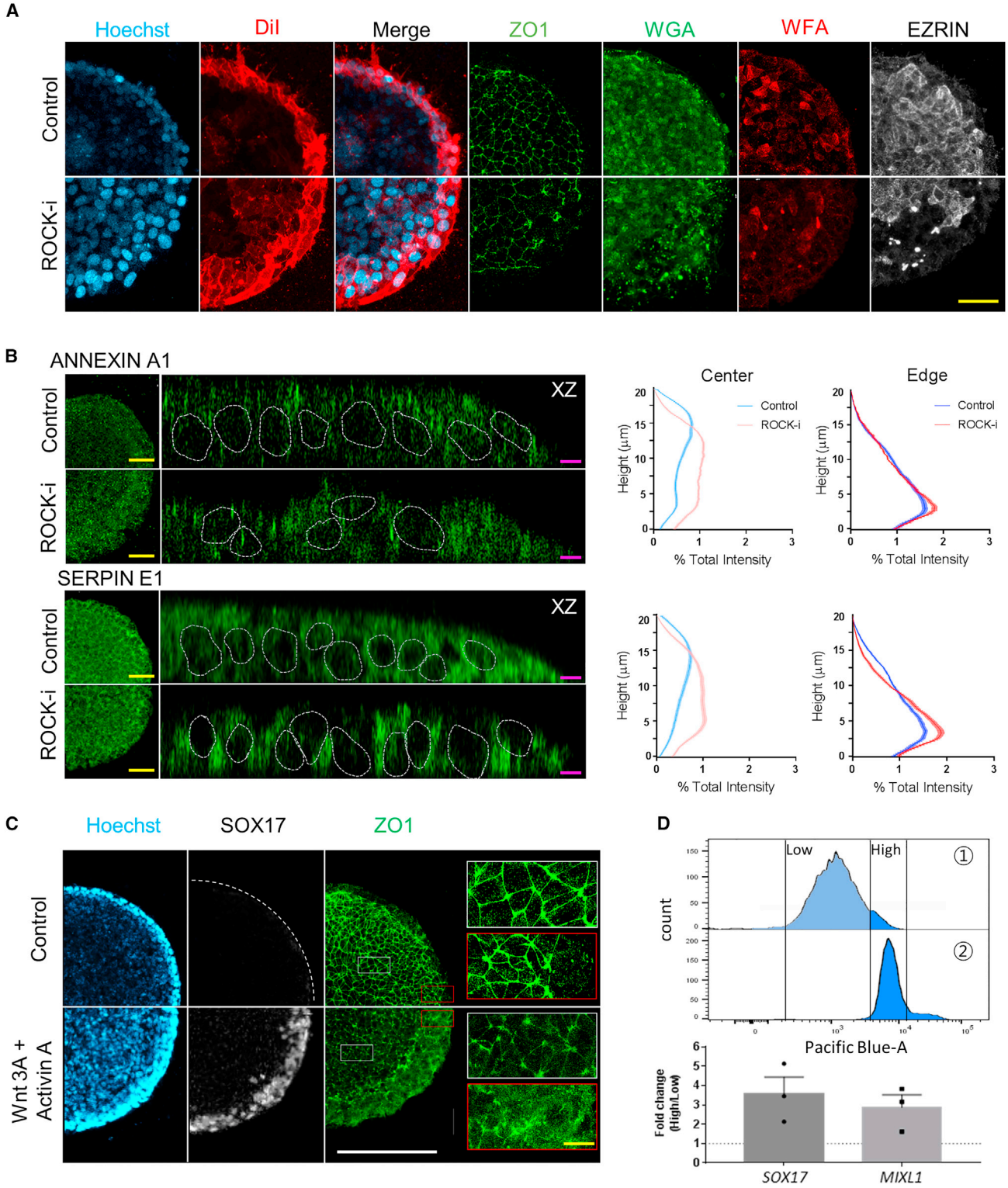

Figure 5. Effect of actin disruption on dye diffusion and apical polarization and characterization of differentiated micropatterned colonies

(A) Micropatterned hPSC colonies were treated with ROCK inhibitor Y-27362 for 24 h. Dye diffusion and apical specialization markers were examined. The top row indicates control groups and the bottom row indicates the ROCK inhibitor treatment group. Y-27632 treatment perturbed polarized distribution of apical markers in the center cells. Scale bar, 50 μm.

(legend continued on next page)

addition to differential mechanical properties that depend on the position within the colony, influence the fate of cells in hPSC colonies (Etoc et al., 2016; Tewary et al., 2017; Warmflash et al., 2014). FA and distinct actin structures have been believed to be fundamental characteristics of hPSCs with pluripotency (Närvä et al., 2017; Stubb et al., 2019). Cells at the border of the colony have different cell-cell adhesion relationships than cells in the center, since one side of the cells at the edge cannot be in contact with other cells, making apico-lateral specialization significantly different at the edge (Théry et al., 2006). These differential cell-ECM or cell-cell adhesions organize the colony edge as a physically distinct region. This positional difference of the colony edge from the center has been proposed as a fundamental mechanism in early embryos executing symmetry breaking and unique differentiation patterning. This feature appears to be recapitulated or strengthened by the geometric confinement of hPSCs on a micropatterned surface *in vitro* (Blin et al., 2018; Deglincerti et al., 2016b). On the other hand, apical specialization in this context has been less addressed so far, and our current study provides new insights that apical specialization, which is dependent on position, causes the differential accessibility of biological and chemical materials.

In our study, we found that different hPSCs exhibited position-dependent differences within colonies in apical specialization in a normal culture, indicating that geometric confinement plays no (or only a marginal) role in the emergence of position-dependent apical specialization. With apicobasal polarization, hPSCs are reported to exhibit microvilli-like structures and glycosylated surface proteins, which are critical factors in apical specialization (Krtolica et al., 2007; Taniguchi et al., 2017). We found that these apical features are virtually absent at the apical domain of the edge cells. In particular, the absence of glycocalyx in the edge cells appears to be important, because glycocalyx is a highly hydrophilic substrate that serves as a physical and chemical barrier for epithelial cells (Möckl, 2020). Considering that the thickness of the glycocalyx affects the permeability of amphiphilic small molecules into the cells (Gao and Lipowsky, 2010; Pikoula et al., 2018), it is tempting to speculate that these differences in apical specialization are involved in position-dependent dye labeling. Several different lines of evidence support this notion. First, not only amphiphilic small compounds, but also hydrophobic DiI labeling, exhibit a position-dependent labeling pattern, suggesting that this differential dye labeling is dependent on the initial contacts of dyes with cell membranes. Second, inhibition of dye-export pumps using specific MDR inhibitors did not affect the position-dependent dye-labeling pattern. Finally, a time course of Hoechst 33342 labeling in the center and edge exhibited similar simple diffusion kinetics exhibiting a gradual increase in intensity. Taken together, it is possible that apical specialization is related to the position-dependent dye labeling.

By taking advantage of differential dye labeling depending on cell position, center and edge cells were separated and for the first time DEG profiles were explored in an unbiased manner. Several classes of genes related to cell migration and cell adhesion or cellular movement were significantly increased in the edge cells (Figures 3 and S4). This finding is consistent with the common view that differences in cell adhesion cause positional differences in the cells. With our own traction force imaging and cell movement analysis, we obtained consistent results showing that the edge of the colony had stronger traction force and higher mobility, which has been shown in early differentiated hESC colonies (Rosowski et al., 2015). This feature reveals the possibility that edge cells stably remain at the edge, even in growing conditions, allowing them to maintain stable topological positions sufficient for the establishment of differential gene expression, and potential symmetry breaking for differentiation with suitable trigger signals. In this context, it is worthy to note that edge and center cells indeed expressed the same level of major pluripotency markers in our condition, suggesting that stemness in both populations is essentially similar. On the contrary, there are reports showing the stem cells with high surface epiblast marker, CD9 (Lau et al., 2020; Nakanishi et al., 2019), or N-cadherin (NCAD) (Nakanishi et al., 2019) preferentially localized at the edge of the cell

(B) The polarized distribution of ANNEXIN A1 and SERPIN E1 in the center cells was disrupted with Y-27632 treatment. Quantification of fluorescence intensity along the z axis (height) in the center and edge cells. In three independent experiments, 26–30 colonies were randomly collected and quantified. Fluorescence intensity at each point was converted into percent total intensity and data represent mean ± SEM. Scale bars, 50 μm (yellow) and 5 μm (magenta).

(C) hPSCs grown on a 500-μm micropattern were treated with Wnt 3A (100 ng/mL) and Activin A (100 ng/mL) for 24 h. Live control and differentiated colonies were labeled with Hoechst and fixed colonies were immunostained with anit-SOX17 and anti-ZO1 antibodies. High-magnification images of boxed areas are shown in the right column. Scale bars, 200 μm (white) and 50 μm (yellow).

(D) Two cell populations upon differentiation were isolated by FACS based on Hoechst labeling intensity (①). To clarify the high-intensity population, dissociated single cells were labeled and analyzed (②). Definitive endoderm marker *SOX17* and *MIXL1* were examined with qPCR analysis using sorted cells. Fold changes (high/low) of indicated genes were calculated. Data represent mean ± SEM in three independent experiments. Each dot represents fold change obtained from an individual batch of experiment (n = 3).

colony. Although we failed to identify the differential gene expression of *CD9* or *NCAD*, we also found that *CAV1* and *EGR1* expression was high in edge cells as NCAD-rich cells in Nakanishi et al.'s study expressed higher levels of *CAV1* and *EGR1* genes (Nakanishi et al., 2019). We currently do not know the exact cause(s) of this discrepancy with other studies regarding pluripotency markers, but it is of importance to note the previous study by Warmflash et al. (2014), which showed that higher expression of pluripotency markers at the colony edge was seen in a 1-mm diameter micropattern, but not in 250-μm or smaller patterns. Considering that we used a 350-μm diameter micropattern, our culture condition appeared to lean to the condition with smaller patterns as in the previous report.

Genes that are highly expressed in edge cells in hPSC colonies appear to be mostly regulated by actin dynamics. In fact, cytoskeleton and polarity proteins have been known to interact reciprocally to establish and maintain cell polarity (Li and Gundersen, 2008; Raman et al., 2018). Accordingly, disruption of actin dynamics with a ROCK inhibitor or actin assembly inhibitors perturbed polarization of apical specialization markers in this study. Interestingly, two DEG genes enriched in the edge cells, *ANNEXIN A1* and *SERPIN E1*, that are not reported to be polarity-dependent molecules in epithelial cells, to our knowledge, were enriched in edge cells at both the mRNA and protein levels, and their distribution was differentially polarized. As cell polarity genes can execute their effects at various levels, ranging from intracellular transport, to cytoskeleton, to cell junctions, to membrane polarity, many unknown molecules could be polarized in hPSCs. ANNEXIN A1, which is known to be involved in EGFR endocytosis, and other endocytosis-related genes, were significantly different between edge and center cells (Grewal et al., 2007; Poeter et al., 2013). Because the localization of endocytosis machinery itself is dependent on cell polarity, it appears that the apical difference between the two cell populations is associated with differential gene expression of related genes and polarity-dependent protein delivery. The change in dye-labeling pattern with actin inhibitors in center cells was strongly correlated with the loss of characteristics of apical domains. These results imply that center cells might acquire edge-like properties upon loss of cell polarity, suggesting the possibility that gene expression profiles could be changed. We believe that it is fair to add cautionary comment that actin polymerization and tight junction assembly are closely related and cannot be functionally segregated, and that actin polymerization inhibitors affected both processes. By using actin inhibitors, therefore, we could not dissect the molecular mechanism, and it is possible that dye uptake and differential gene expression at center cells is more associated with sealed epithelium, as shown in previous studies (Etoc et al., 2016).

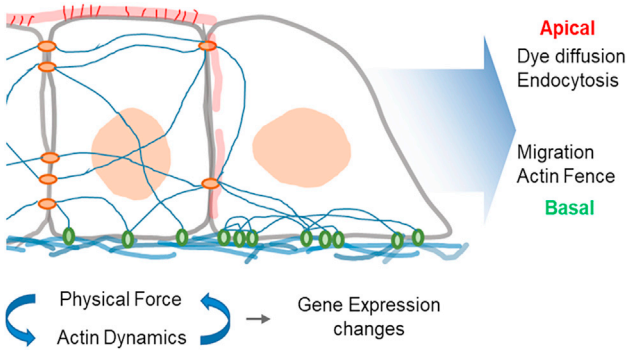

Figure 6. Diagram of position-dependent differences in hPSC colonies and relevant contribution to biological functions

Differential mechanical force and actin dynamics in edge and center cells induce differential gene expression profiles in hPSC colonies, leading to position-dependent differences in biological functions including endocytosis, dye diffusion, migration, and actin fence formation.

In conclusion, position-dependent features, such as mechanical force and actin dynamics, might induce differential gene expression profiles in hPSC colonies depending on position. These differences lead to establishment of differential cellular polarity in center and edge cells, which creates position-dependent differences in biological functions including endocytosis, dye diffusion, migration, and actin fence formation (Figure 6). Finally, these position-dependent properties might affect responses of hPSCs to morphogens or other stimuli, resulting in symmetry breaking to fate determination.

EXPERIMENTAL PROCEDURES

For further details, see supplemental experimental procedures.

Master fabrication and micro-contact printing

Polydimethylsiloxane stamp production and micro-contact printing was executed as reported previously (Ryu et al., 2016), and a summary diagram for the procedure is presented in Figure 1A.

Cell culture

The hPSC study was approved by the Korea University institutional review board. hPSCs (H9, H1, hiPSC no. 5-1, ZO1_EGFP hiPSC lines) were grown on a tissue culture dish coated with diluted Matrigel (Corning, 354277; 1:25 in DMEM/F12), and maintained with mTesR1 (STEMCELL Technologies) medium.

Live cell fluorescence dye staining

Cells grown on micropatterned substrates were briefly washed with HBSS and incubated with dyes for 15 min.

Drug treatments

Drugs were treated for 20 min before dye staining. ROCK inhibitor Y27362 (Tocris no. 1254, 10 μM) was treated for 24 h before dye staining or fixation. Latrunculin B (2 μM, Sigma) and cytochalasin D (50 nM, Sigma) were treated for 1 h before dye staining or fixation.

Image analysis and statistical analysis

Every experiment was repeated three to five times. In each batch of experiment, eight to ten colonies were used for quantification. Statistical analysis was performed using GraphPad Prism 7.0 software.

Quantitative analysis of kinematics and mechanical dynamics of hPSC colonies

To measure the movement and physical force of the cell colony, we used the same method as in our previous works (Jang et al., 2017).

Immunocytochemistry and lectin labeling

For immunocytochemistry, cells were fixed with 4% paraformaldehyde for 15 min at 25°C and submersed in the blocking solution (3% BSA and 0.2% Triton X-100 in 1× PBS) for 30 min. Then, cells were treated with blocking solution and primary antibodies at 4°C overnight. The next day, the cells were incubated in an appropriate secondary antibody.

SEM

The hPSCs were seeded on a micropatterned 12-mm Ø coverslip in a 12-well plate for SEM imaging.

FACS analysis

After dye staining, edge (high) and center (low) cells were purified using a flow cytometer sorter (FACSAriaIII, PE-A laser).

RNA-seq and data analysis

Total RNA was extracted from nine samples using TRIzol reagent. First-strand cDNA was synthesized from the fragmented mRNA using SuperScript II reverse transcriptase (Invitrogen, no. 18064014) and random primers. DNA polymerase I, RNase H, and dUTP were used for second-strand cDNA synthesis. Indexed libraries were sequenced using an Illumina NovaSeq (Illumina, San Diego, CA, USA) and the paired-end (2× 100 bp) sequencing was done by Macrogen. Nine samples were used for transcriptome analysis with edgeR.

Laser microdissection microscopy

Cells were cultured on micropatterned polyethylenenaphthalate membrane (Leica, no. 11600289). Edge and center cells were cut with a laser under laser microdissection microscopy (LMD6, Leica) in live state (Podgorny, 2013) and collected in a PCR tube (PCR-02-C, Axygen). Then, each sample was used for qPCR analysis.

qPCR

All the cDNA samples were generated using a SuperScript IV CellDirect cDNA synthesis Kit (11750150, Invitrogen). qPCR was performed using a QuantStudio 3 Real-Time PCR system.

Fluorescence *in situ* hybridization

The probes used in this study were purchased from Advanced Cell Diagnostics (Hayward, CA).

Data and code availability

The accession code of the sequencing data used in this study is SRA database: PRJNA757524.

SUPPLEMENTAL INFORMATION

Supplemental information can be found online at https://doi.org/10.1016/j.stemcr.2021.11.005.

AUTHOR CONTRIBUTIONS

Conceptualization, J.R. and W.S.; methodology, Y.K., B.L., H.M.C., E.Y., and H.K.; software, J.-A.G., H.J., J.H.K., and Y.P.; formal analysis, Y.K., H.J., and H.J.K.; investigation, Y.K., H.J., and K.S.; writing – original draft, Y.K., J.R.R., and W.S.; writing – review & editing, Y.K., J.R., and W.S.; supervision, W.S. and J.R.

CONFLICT OF INTEREST

The authors declare no competing interests.

ACKNOWLEDGMENTS

This research was funded by the National Research Foundation of Korea (NRF) grant funded by the Korea government (MSIP) (NRF-2019M3D1A1078940, NRF-2017M3A9B3061308, NRF-2017M3C7A1047654, and NRF-2016R1D1A1B01011346). We thank Hyun-Wook Kim for sample preparation and imaging with a scanning electron microscope and Eun-Ok Kim for FACSAriaIII sorting at the Medical Science Research Center.

Received: August 31, 2020
Revised: November 12, 2021
Accepted: November 15, 2021
Published: December 16, 2021

REFERENCES

Blin, G., Wisniewski, D., Picart, C., Thery, M., Puceat, M., and Lowell, S. (2018). Geometrical confinement controls the asymmetric patterning of Brachyury in cultures of pluripotent cells. Development *145*, dev166025.

Deglincerti, A., Etoc, F., Ozair, M.Z., and Brivanlou, A.H. (2016a). Chapter six—self-organization of spatial patterning in human embryonic stem cells. In Current Topics in Developmental Biology, P.M. Wassarman, ed. (Academic Press), pp. 99–113.

Deglincerti, A., Etoc, F., Guerra, M.C., Martyn, I., Metzger, J., Ruzo, A., Simunovic, M., Yoney, A., Brivanlou, A.H., Siggia, E., et al. (2016b). Self-organization of human embryonic stem cells on micropatterns. Nat. Protoc. *11*, 2223–2232.

Etoc, F., Metzger, J., Ruzo, A., Kirst, C., Yoney, A., Ozair, M.Z., Brivanlou, A.H., and Siggia, E.D. (2016). A balance between secreted inhibitors and edge sensing controls gastruloid self-organization. Dev. Cell *39*, 302–315.

Florian, M.C., and Geiger, H. (2010). Concise review: polarity in stem cells, disease, and aging. Stem Cells *28*, 1623–1629.

Gao, L., and Lipowsky, H.H. (2010). Composition of the endothelial glycocalyx and its relation to its thickness and diffusion of small solutes. Microvasc. Res. *80*, 394–401.

Green, M.D., Chen, A., Nostro, M.-C., d'Souza, S.L., Schaniel, C., Lemischka, I.R., Gouon-Evans, V., Keller, G., and Snoeck, H.-W. (2011). Generation of anterior foregut endoderm from human embryonic and induced pluripotent stem cells. Nat. Biotechnol. *29*, 267–272.

Grewal, T., Hegemann, A., Vila, S., and Enrich, C. (2007). Annexins regulate EGFR signaling and trafficking. Calcium Bind. Proteins *2*, 11–20.

Heemskerk, I., and Warmflash, A. (2016). Pluripotent stem cells as a model for embryonic patterning: from signaling dynamics to spatial organization in a dish: stem cells as a model for embryonic patterning. Dev. Dyn. *245*, 976–990.

Hilbig, H., Bidmon, H.J., Blohm, U., and Zilles, K. (2001). *Wisteria floribunda* agglutinin labeling patterns in the human cortex: a tool for revealing areal borders and subdivisions in parallel with immunocytochemistry. Anat. Embryol. *203*, 45–52.

Jang, H., Notbohm, J., Gweon, B., Cho, Y., Park, C.Y., Kee, S.-H., Fredberg, J.J., Shin, J.H., and Park, Y. (2017). Homogenizing cellular tension by hepatocyte growth factor in expanding epithelial monolayer. Sci. Rep. *7*, 45844.

Krtolica, A., Genbacev, O., Escobedo, C., Zdravkovic, T., Nordstrom, A., Vabuena, D., Nath, A., Simon, C., Mostov, K., and Fisher, S.J. (2007). Disruption of apical-basal polarity of human embryonic stem cells enhances hematoendothelial differentiation. Stem Cells *25*, 2215–2223.

Lahmy, S., Viallet, P., and Salmon, J.M. (1995). Is reduced accumulation of Hoechst 33342 in multidrug resistant cells related to P-glycoprotein activity? Cytometry *19*, 126–133.

Lau, K.X., Mason, E.A., Kie, J., De Souza, D.P., Kloehn, J., Tull, D., McConville, M.J., Keniry, A., Beck, T., Blewitt, M.E., et al. (2020). Unique properties of a subset of human pluripotent stem cells with high capacity for self-renewal. Nat. Commun. *11*, 2420.

Li, R., and Gundersen, G.G. (2008). Beyond polymer polarity: how the cytoskeleton builds a polarized cell. Nat. Rev. Mol. Cell Biol. *9*, 860–873.

Ma, Z., Wang, J., Loskill, P., Huebsch, N., Koo, S., Svedlund, F.L., Marks, N.C., Hua, E.W., Grigoropoulos, C.P., Conklin, B.R., et al. (2015). Self-organizing human cardiac microchambers mediated by geometric confinement. Nat. Commun. *6*, 7413.

Martyn, I., Kanno, T.Y., Ruzo, A., Siggia, E.D., and Brivanlou, A.H. (2018). Self-organization of a human organizer by combined Wnt and Nodal signalling. Nature *558*, 132–135.

Möckl, L. (2020). The emerging role of the mammalian glycocalyx in functional membrane organization and immune system regulation. Front. Cell Dev. Biol. *8*, 253.

Monsigny, M., Roche, A.-C., Sene, C., Maget-Dana, R., and Delmotte, F. (1980). Sugar-lectin interactions: how does wheat-germ agglutinin bind sialoglycoconjugates? Eur. J. Biochem. *104*, 147–153.

Nakanishi, M., Mitchell, R.R., Benoit, Y.D., Orlando, L., Reid, J.C., Shimada, K., Davidson, K.C., Shapovalova, Z., Collins, T.J., Nagy, A., et al. (2019). Human pluripotency is initiated and preserved by a unique subset of founder cells. Cell *177*, 910–924.e22.

Närvä, E., Stubb, A., Guzmán, C., Blomqvist, M., Balboa, D., Lerche, M., Saari, M., Otonkoski, T., and Ivaska, J. (2017). A strong contractile actin fence and large adhesions direct human pluripotent colony morphology and adhesion. Stem Cell Reports *9*, 67–76.

Orozco-Fuentes, S., Neganova, I., Wadkin, L.E., Baggaley, A.W., Barrio, R.A., Lako, M., Shukurov, A., and Parker, N.G. (2019). Quantification of the morphological characteristics of hESC colonies. Sci. Rep. *9*, 17569.

Pikoula, M., Tessier, M.B., Woods, R.J., and Ventikos, Y. (2018). Oligosaccharide model of the vascular endothelial glycocalyx in physiological flow. Microfluid. Nanofluid. *22*, 21.

Podgorny, O.V. (2013). Live cell isolation by laser microdissection with gravity transfer. J. Biomed. Opt. *18*, 055002.

Poeter, M., Radke, S., Koese, M., Hessner, F., Hegemann, A., Musiol, A., Gerke, V., Grewal, T., and Rescher, U. (2013). Disruption of the annexin A1/S100A11 complex increases the migration and clonogenic growth by dysregulating epithelial growth factor (EGF) signaling. Biochim. Biophys. Acta *1833*, 1700–1711.

Raman, R., Pinto, C.S., and Sonawane, M. (2018). Polarized organization of the cytoskeleton: regulation by cell polarity proteins. J. Mol. Biol. *430*, 3565–3584.

Reily, C., Stewart, T.J., Renfrow, M.B., and Novak, J. (2019). Glycosylation in health and disease. Nat. Rev. Nephrol. *15*, 346–366.

Romito, A., and Cobellis, G. (2016). Pluripotent stem cells: current understanding and future directions. Stem Cells Int. *2016*, 9451492.

Rosowski, K.A., Mertz, A.F., Norcross, S., Dufresne, E.R., and Horsley, V. (2015). Edges of human embryonic stem cell colonies display distinct mechanical properties and differentiation potential. Sci. Rep. *5*, 1–12.

Ryu, J.R., Jang, M.J., Jo, Y., Joo, S., Lee, D.H., Lee, B.Y., Nam, Y., and Sun, W. (2016). Synaptic compartmentalization by micropatterned masking of a surface adhesive cue in cultured neurons. Biomaterials *92*, 46–56.

Simunovic, M., and Brivanlou, A.H. (2017). Embryoids, organoids and gastruloids: new approaches to understanding embryogenesis. Development *144*, 976–985.

Stubb, A., Guzmán, C., Närvä, E., Aaron, J., Chew, T.-L., Saari, M., Miihkinen, M., Jacquemet, G., and Ivaska, J. (2019). Superresolution architecture of cornerstone focal adhesions in human pluripotent stem cells. Nat. Commun. *10*, 4756.

Taniguchi, K., Shao, Y., Townshend, R.F., Cortez, C.L., Harris, C.E., Meshinchi, S., Kalantry, S., Fu, J., O'Shea, K.S., and Gumucio, D.L. (2017). An apicosome initiates self-organizing morphogenesis of human pluripotent stem cells. J. Cell Biol. *216*, 3981–3990.

Tewary, M., Ostblom, J., Prochazka, L., Zulueta-Coarasa, T., Shakiba, N., Fernandez-Gonzalez, R., and Zandstra, P.W. (2017). A stepwise model of reaction-diffusion and positional information governs self-organized human peri-gastrulation-like patterning. Development *144*, 4298–4312.

Théry, M. (2010). Micropatterning as a tool to decipher cell morphogenesis and functions. J. Cell Sci. *123*, 4201–4213.

Théry, M., Racine, V., Piel, M., Pépin, A., Dimitrov, A., Chen, Y., Sibarita, J.-B., and Bornens, M. (2006). Anisotropy of cell adhesive microenvironment governs cell internal organization and orientation of polarity. Proc. Natl. Acad. Sci. U S A *103*, 19771–19776.

Thomson, J.A., Itskovitz-Eldor, J., Shapiro, S.S., Waknitz, M.A., Swiergiel, J.J., Marshall, V.S., and Jones, J.M. (1998). Embryonic stem cell lines derived from human blastocysts. Science *282*, 1145–1147.

Warmflash, A., Sorre, B., Etoc, F., Siggia, E.D., and Brivanlou, A.H. (2014). A method to recapitulate early embryonic spatial patterning in human embryonic stem cells. Nat. Met. *11*, 847–854.

Xue, X., Sun, Y., Resto-Irizarry, A.M., Yuan, Y., Yong, K.M.A., Zheng, Y., Weng, S., Shao, Y., Chai, Y., Studer, L., et al. (2018). Mechanics-guided embryonic patterning of neuroectoderm tissue from human pluripotent stem cells. Nat. Mater. *17*, 633–641.

Zhou, S., Schuetz, J.D., Bunting, K.D., Colapietro, A.-M., Sampath, J., Morris, J.J., Lagutina, I., Grosveld, G.C., Osawa, M., Nakauchi, H., et al. (2001). The ABC transporter Bcrp1/ABCG2 is expressed in a wide variety of stem cells and is a molecular determinant of the side-population phenotype. Nat. Med. *7*, 1028–1034.